JSAE 20239087
SAE 2023-32-0054

The influence of fluid properties on near nozzle sprays in clean and fouled GDI injectors

Alex Gander, Guillaume de Sercey, Cyril Crua
Advanced Engineering Centre, University of Brighton, Brighton, UK

ABSTRACT

Physical fluid properties and GDI injector deposits are known to impact the internal nozzle flow and external spray morphology. Furthermore, deposits can affect injector calibration and damage the delicate mixing and combustion processes. Despite this, there is a lack of experimental data demonstrating the discrete influence of fluid properties and how this influence evolves with the formation of injector deposits. This article aims to further the existing knowledge on the effect of fluid properties such as density, kinematic viscosity and surface tension, along with distillation on fuel spray characteristics and provide insight into how sprays change over the lifetime of GDI injectors due to fouling. In this investigation, four gasoline fuels with varying concentrations of ethanol and typical GDI additive, including one being representative of a renewable gasoline formulation, were used with clean and fouled multi-hole GDI fuel injectors. A low-pressure constant-volume chamber was used to produce a controlled inert atmosphere at various ambient and injection conditions. Shadowgraph images were recorded using two high-speed cameras at the micro and macro scales to simultaneously visualise the fluid dynamic processes in the near nozzle and downstream regions. Image analysis demonstrated that fouling had a significant impact on the spray angle. Standard error of the mean was used to determine the repeatability of the measurements taken, and it was found that the spray width at the nozzle tip had a very low standard error. In contrast, a comparatively high standard error was calculated for spray dispersion angle exhibited for the fouled and clean injectors. Due to high repeatability on spray width measurements, positive correlations were found between the spray width at the nozzle tip and initial boiling point, surface tension and kinematic viscosity, and negative correlations with density and final boiling point.

INTRODUCTION

Gasoline direct injection (GDI) engines have been favoured over port fuel injection (PFI) engines for several years now due to their higher level of precision in fuel delivery and combustion, which ultimately results in higher fuel economy and lower pre-catalyst emissions [1]. Due to the high precision required to produce the low emission levels set out by legislators, there is a significant challenge in keeping the entire system in a steady condition to prevent the deviation of both the injection and combustion events from the original calibration. Two variables that influence the spray and combustion characteristics are the development of fuel injector deposits and a change in the physical properties of the fuel [2, 3]. These characteristics will become increasingly influenced by injector deposits over the lifespan of the fuel injector due to the effective orifice diameter becoming smaller and restricting mass flow rate, with examples of deposits being shown in Figure 1 [4].

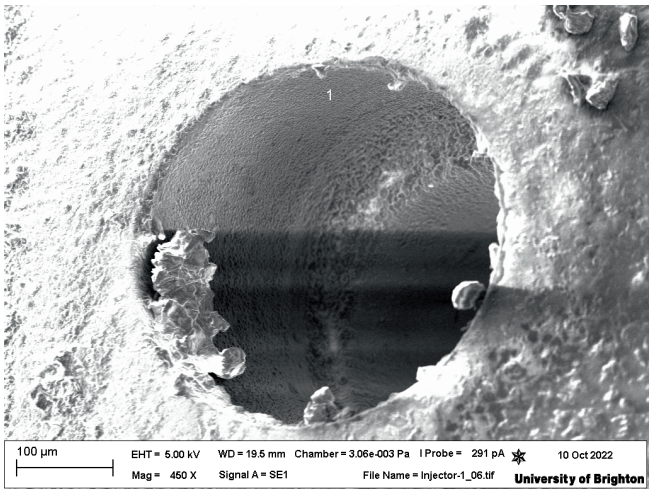

Figure 1: Injector deposits in and around a multi-hole GDI injector orifice.

A study on the influence of injector deposits on engine performance and spray morphology across multiple commercially available GDI fuel injectors highlighted two common issues at both non-boiling and flashboiling conditions: a decrease in spray angle and increased likelihood of spray collapse [2]. Although, some studies such as [5] and [6] are contradictory, demonstrating, a decrease and increase in penetration, respectively. This difference could be due to the slight variations in operating conditions or the severity of the injector nozzle fouling [5, 6]. Regardless of the changes in the spray characteristics due to fuel in-

jector deposits, it has been well established that they significantly impact the production of pre-catalyst engine emissions, with rises in PN/PM and unburnt hydrocarbons being most notable [6, 7]. In contrast to the influence of injector deposits on GDI sprays and combustion, the literature on the influence of physical fluid properties on GDI spray characteristics is limited [8]. From what has been published, it is known that physical fluid properties do have a subtle influence over spray characteristics, as Ulrich et al. demonstrate when comparing water and ethanol sprays using 2p-LIF [8]. It was found that the higher dynamic viscosity of ethanol will produce a greater spray angle which is consistent with the basic model presumption by Zigan et al. which also notes a decrease in spray penetration [8, 9]. Computational fluid dynamics has also been used to evaluate the influence of physical fluid properties on GDI spray characteristics, with an LES-VOF model used by Yue and Som, 2022 predicted an increase in injection velocity and lower mass flow rate at the nozzle exit when comparing isooctane to ethanol which has a lower density and viscosity [3]. However, by the time the spray reaches the counterbore exit, the spray velocity difference is negligible [3]. Due to the lack of experimental data available on the influence of fluid properties, this study aims to provide insight into how this effect may alter over the life span of the injector. Simultaneous shadowgraph measurements were taken using two high-speed monochromatic cameras with micro and macroscopic lenses inside a temperature-controlled constant volume low-pressure spray chamber. Four gasoline fuels with varying concentrations of ethanol and typical GDI additive, including one representative of a renewable gasoline formulation, were used with clean and fouled fuel injectors. Image processing was then used to extract spray angle, width and penetration. This article is divided into three main components, including the introduction. The second section discusses the methodology and post-processing method and the fuel's physical fluid properties. The third section presents the results from the study evaluating the influence of physical fuel properties on spray width, angle and penetration, which are then compared to the same measurements from a fouled injector. Finally, the key findings from the experiments are detailed in the conclusion.

EXPERIMENTAL METHODS

Constant volume spray chamber

Optical spray data was collected in a hexagonal low-pressure constant volume chamber (Figure 2), which allows for a high level of optical access and thermal stability compared to an optical engine. Two proportional–integral–derivative (PID) control systems regulate the thermal boundary conditions for the internal chamber and injector nozzle temperature with maximum temperatures of 60 and 120 °C, respectively. Nitrogen is used to keep the internal atmosphere of the chamber inert, with the chamber purged frequently using a rotary vane vacuum pump to remove any air or fuel introduced to the system during spray tests. Maximum chamber gas pressure is 1.1 bar absolute which is monitored by a pressure transducer and regulated by a controllable pressure regulator with the nitrogen supply from a gas bottle. Pressure is set in the chamber by purging the system using the vacuum pump and leaking in nitrogen with the controllable regulator set to the desired ambient pressure. Chamber boundary conditions are monitored and logged by a National Instruments cRIO system using in-house developed LABVIEW software at a log rate of 10 Hz.

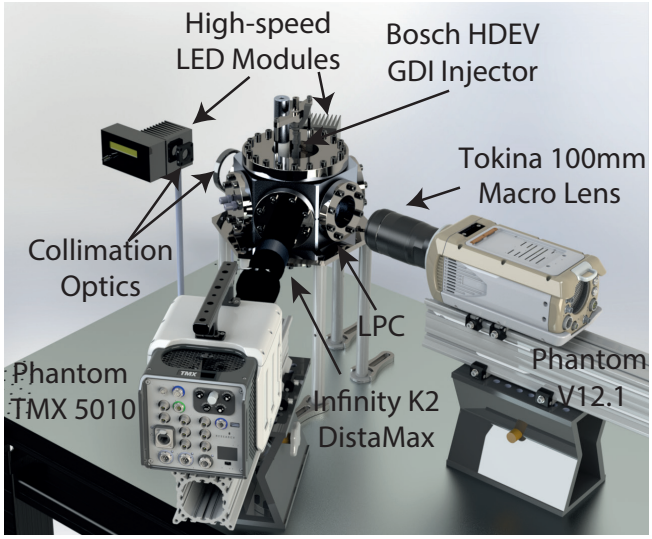

Figure 2: Experimental setup of low pressure constant volume optical chamber

Fuel system

The fuelling and injection parameters are controlled by the same in-house software used for data logging and controlling chamber pressure. This software manages the number of injection events, electronic trigger and dwell period. Injector control parameters, such as control voltage, are managed via a custom injector driver. Table 1 shows the fuel injection parameters used for this study. Fuel delivery to the injector was handled by a Teledyne ISCO 240HP syringe pump with high-pressure tubing carrying the fuel from the pump to the injector with a maximum operating pressure of 655 bar with an accuracy of 0.5 % of full scale. The data logging also provides overall system control including fuel injection parameters. The fuel line has a 5 micron in-line filter on the intake for filling the pump and inline. The fuel injector used was a Bosch HDEV5 multi-hole GDI injector operated at 200 bar gauge pressure with an electronic injection duration of 780 µs. The electronic injection duration and triggering was controlled by a custom in-house national instruments injection driver which sends the control voltages to the injector once the trigger is received from the control system for the entire test system.

Table 1: Experimental injection parameters

Injection pressure	20 MPa
Injection duration	780 µs
Injection dwell period	333 µs
Injection events per log	10 (Fouled), 20 (Clean)
Chamber Temperature	333 K
Injector Temperature	333 K

Fuel injectors

Two Bosch HDEV 5.2 GDI fuel injectors were used for the study. One was used in engine for a prolonged period and the other used out of engine only in a spray rig for calibration tests. The fouled injector shown in Figure 3 was run in engine for approximately 4000 km on a high-octane gasoline fuel before use for testing in this study. The clean injector from Figure 3 was used for out of engine tests in a spray rig using a calibration fluid and was cleaned with acetone prior to testing to help clear any residue left over from previous spray tests. SEM images were also captured from each hole to gain insight to how far the internal geometry had been compromised due to deposit growth. Figure 1 shows internal deposits which are representative of what is seen in all of the other holes in the injector, except for the centre hole where significantly fewer internal deposits were seen.

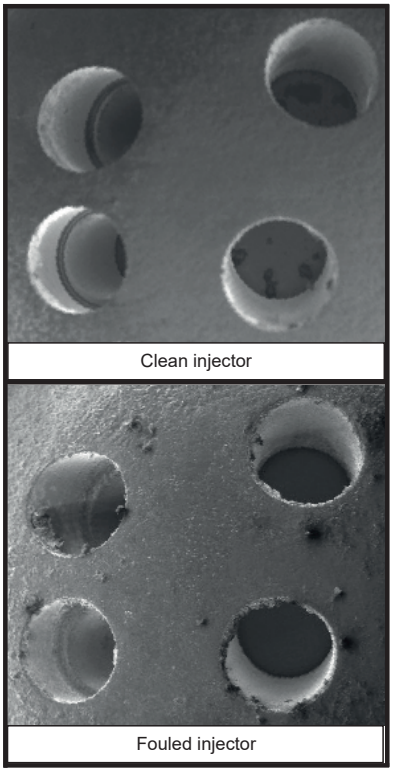

Figure 3: Scanning electron microscopy images of the injectors used for the study. The fouled injector was fouled over approximately 4000 km of engine running.

Fuels

The study uses four multi-component fuels of varying composition in order to generate changes in physical property profiles. For this we used gasoline fuels with 0 (E0) and 10 % (E10) ethanol content as well as an E10 gasoline with a typical GDI additive, and a blend which is representative of a fully renewable blend, which is described as "Renewable Proxy" in the results section. Their initial boiling point (IBP), 50 % distillation and final boiling point (FBP) are given in Table 2 and describe the amount of fuel distilled as a percentage of the initial mass with FBP being 100 % distilled. Table 2 also shows the measured physical properties of the fuels used in the study. Property measurements were taken at a range of non-evaporative conditions, with the values given being the highest of the temperatures at which the measurements were taken to more accurately represent the fuel's properties throughout testing.

Optical configuration

Image data of the fuel spray was captured using a Phantom TMX 5010 and V12.1 high-speed cameras, with a BSI and CMOS sensor respectively. All recordings captured and saved using the manufacturer provided software.

Both high-speed cameras were operated simultaneously to capture the macroscopic and microscopic spray regions concurrently. The Phantom TMX 5010 ran at a frame rate of 66 kHz with a 95 ns exposure time to eliminate motion blurring at a resolution of 1024 $\times$ 608 pix^2. The Phantom V12.1 was operated at 14 kHz with an exposure time of 500 ns at a resolution of 640 $\times$ 640 pix^2. A full list of optical and capture settings is given in Figure 3. Both imaging setups used the high-speed cameras to pulse custom high-speed LED drivers at the stated frame rates. The LED drivers were fitted with 460 nm blue LEDs which had a measured optical rise time of 20 ns, collimation optics and optical diffusers to provide a homogenous background. LED brightness was controlled by tuning the LED supply voltage.

Table 3: Recording and optical setup

Image scale	Micro	Macro
Camera	Phantom TMX 5010	Phantom V12.1
Sensor	BSI	CMOS
Frame rate	66 kHz	14 kHz
Exposure time	95 ns	2 µs
Lens	Infinity K2 Distamax CF-3	Tokina atx-i 100mm
Aperture	50%	f/2.8
Scale Factor	8.96 µm/pix	76 µm/pix

Table 2: Physical fluid properties of the fuels used in the study. Surface tension measurement accuracy is ±2%

Parameter	E0	E10	E10 without GDI additive	Renewable
Density at 15 °C [kg/L]	0.7425	0.7460	0.7447	0.7534
Kinematic Viscosity at 40 °C [mm^2/s]	0.5294	0.5460	0.5240	0.5020
Surface Tension at 35 °C [mN/m]	20.3	20	19.9	19
IBP / 50% Distillation / FBP [°C]	47.4 / 58.6 / 138.4	44.7 / 51.9 / 136	44.4 / 51.7 / 133.5	27.5 / 97 / 206.6

Post-processing

Optical spray data were saved as individual spray events to obtain quantitative results from the raw optical spray and processed using MATLAB. Image processing was then used to remove any non-homogeneities from the image background. All frames before the injection event were used to flatfield the remainder of the recording. After processing, an image mask was created to prevent any measurement artefacts generated by the chamber hardware or injector nozzle. Spray width is taken as the first and last pixel of the largest object on a specified plane. The spray angle is measured by finding the left and right edges of the spray region between two pre-defined planes with a linear fit performed on each edge. The coefficients from the linear fit are then used to compute the left and right outer plume angle which are then added together to produce the full outer plume angle. Figure 4 details which planes and regions are used for computing width and angle measurements. Once the measurements for each spray event were obtained, the mean, standard deviation and standard error of the steady state period were calculated.

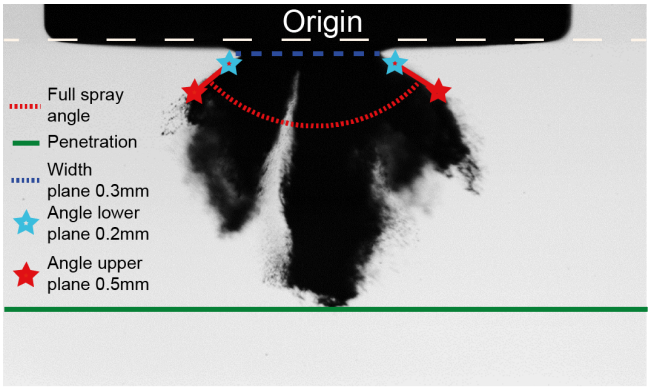

Figure 4: Schematic describing the measurement planes and regions used to compute spray width and angle measurements. The origin is defined as the row where the radius around the edge of the injector becomes flat.

This article will use the following definition of the steady-state period: the moment where the spray is fully formed after the initial stages of the hydraulic injection period to just before the moment the injection pressure begins to fall as the needle starts to close, visualised in Figure 5. For these calculations 10 experimental repeats were captured for the fouled injector and 20 for the clean injector. These mean values were then plotted against fluid properties to determine their effect, with the standard error used as error bars.

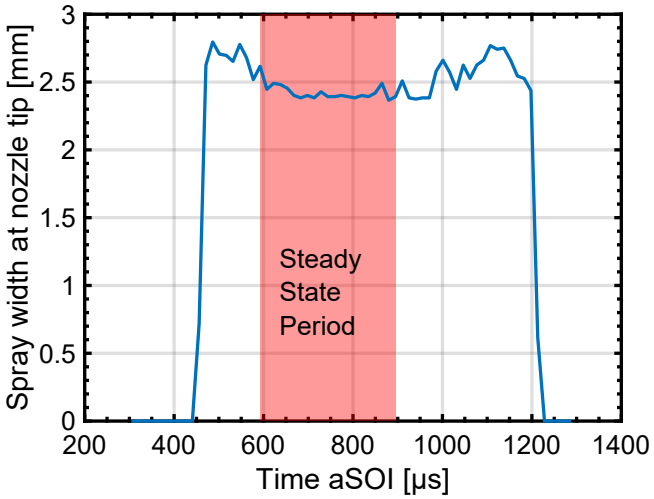

Figure 5: Illustration demonstrating the steady state spray period used for measurements. Test point used for illustration is E0 fuel at 20 MPa fuel pressure, 333 k ambient and nozzle temperature and 1000 mbar atmospheric pressure

RESULTS

The results below were achieved using the previously discussed methodology and changes in fuel to invoke a change in physical fluid properties. It is important to note that the start and end of the injection are both taken from the same spray event and are deemed representative of the other recordings captured within the set. Firstly Figure 6, shows qualitative sequences of the start and end of injection in the microscopic view comparing the clean and fouled injectors. To discuss the start of injection first, the second row in Figure 6 is the first to demonstrate significant differences between the clean and fouled injectors, with gaps opening up on opposite sides of the spray plume. This result was unexpected, and so, the orientation of the injectors was investigated to confirm the orientation of the injectors

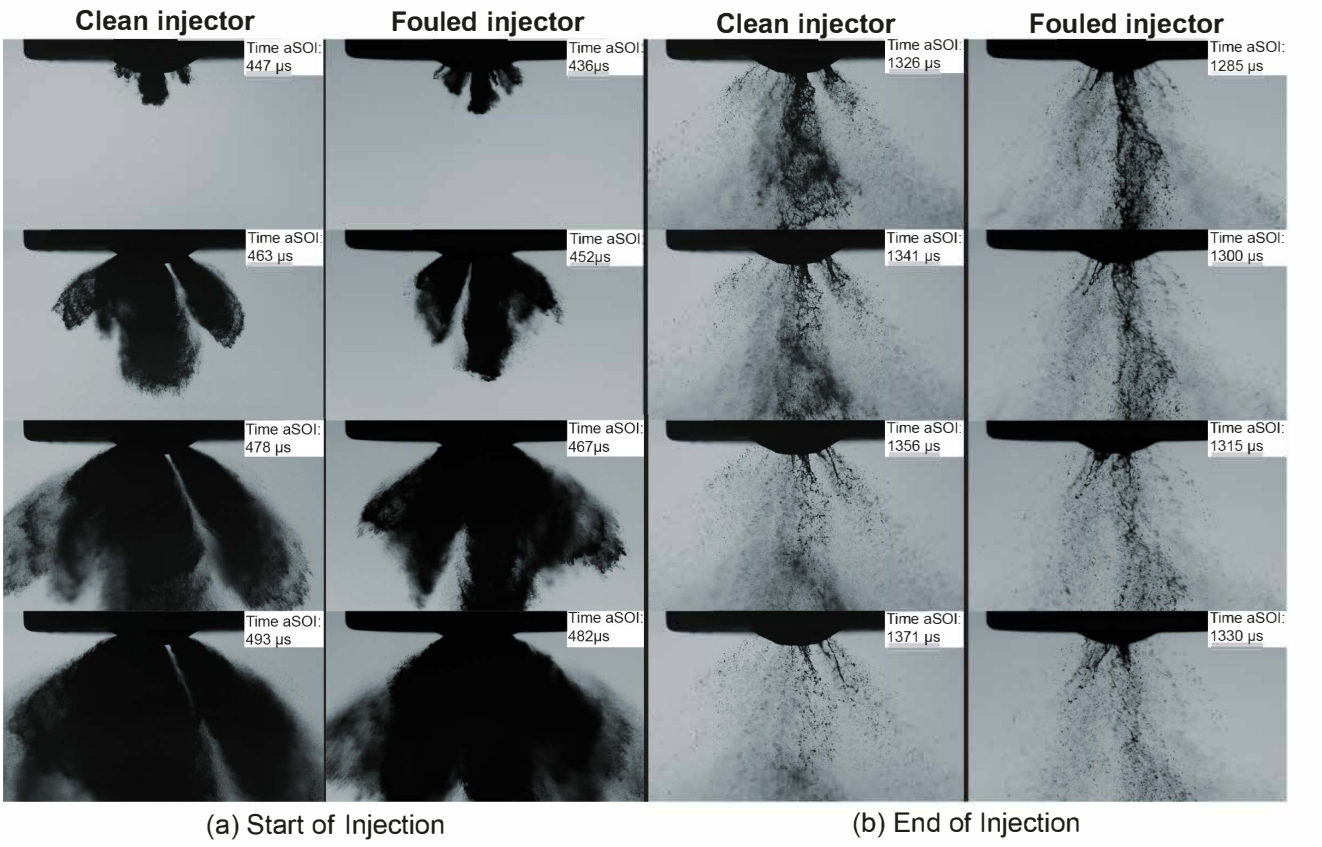

Figure 6: Comparison of clean and fouled sprays at start (Left) and end (Right) of hydraulic injection using the E0 gasoline at 200 bar injection pressure, 333 K injector and chamber temperature.

was identical, as intended. Now comparing the two results from Figure 6 the overall spray from the fouled injector appears under-expanded in terms of spray area as compared to that of the clean injector. This draws parallels to the discussion in the introduction of this article with other reports highlighting that the presence of injector deposits typically induce a reduction in overall spray angle [2]. This reduction in the overall plume angle logically suggests a reduction in the individual plume angle which would explain the appearance of a new gap in the spray plume.

However, this does not explain the appearance of a gap on the opposite side of the plume when using a clean injector. One explanation for this could be that deposit growth around the counter-bore orifices is inconsistent, leading to some counter-bore rims having larger deposits than others, as shown in Figure 3. This change in the size of the deposits formed will influence the fuel spray's interaction with the injector nozzle, possibly pulling fluid in one direction. However, these hypotheses would need to be investigated in future works using high magnification and a different optical configuration to that used in this study. When discussing the end of injection (EOI) on the right side of Figure 6 it appears that the presence of deposits is inhibiting atomisation with longer ligaments when comparing the two sprays at 1341 µs and 1300 µs for the clean and fouled spray respectively. Figure 7a shows the influence of the different fuels on the initial stages of fuel injection. For this comparison, the frame sequences shown were synchronised by finding the first frame where the fuel was present. In this case, the first frames were within 2 µs of each other. Looking at the first row of Figure 7a, which depicts the first sight of fuel being ejected from the nozzle at approximately 448 µs aSOI, there are broad similarities, with the renewable proxy fuel being the only one that is not yet displaying distinct individual plumes, unlike the ethanol fuels. However, if we consider the 2 µs time difference between them from the start of the injection trigger, they all could be similar enough at this stage. Moving to the second row of Figure 7a, all fuels exhibit a distinct stand-alone spray plume on the right of the spray. On the left of the spray is where differences start to become apparent, with the ethanol fuels seemingly demonstrating an increased axial penetration over the renewable proxy. Furthermore, the E10 fuel displays a greater readiness to atomise in the lower left part of the spray plume when compared to the E0 and renewable proxy. This increased readiness could be accredited to the slightly lower distillation characteristic and surface tension of the E10 fuels, meaning the fuel is vaporising more easily and producing smaller, more dispersed droplets. However, a more in-depth study into accurate drop sizing is required to confirm or deny this. Moving to rows three and four of Figure 7a, show very similar fuel sprays for all the ethanol fuels, whereas the renewable proxy looks quite different and is struggling to develop on the left-hand side of the spray plume.

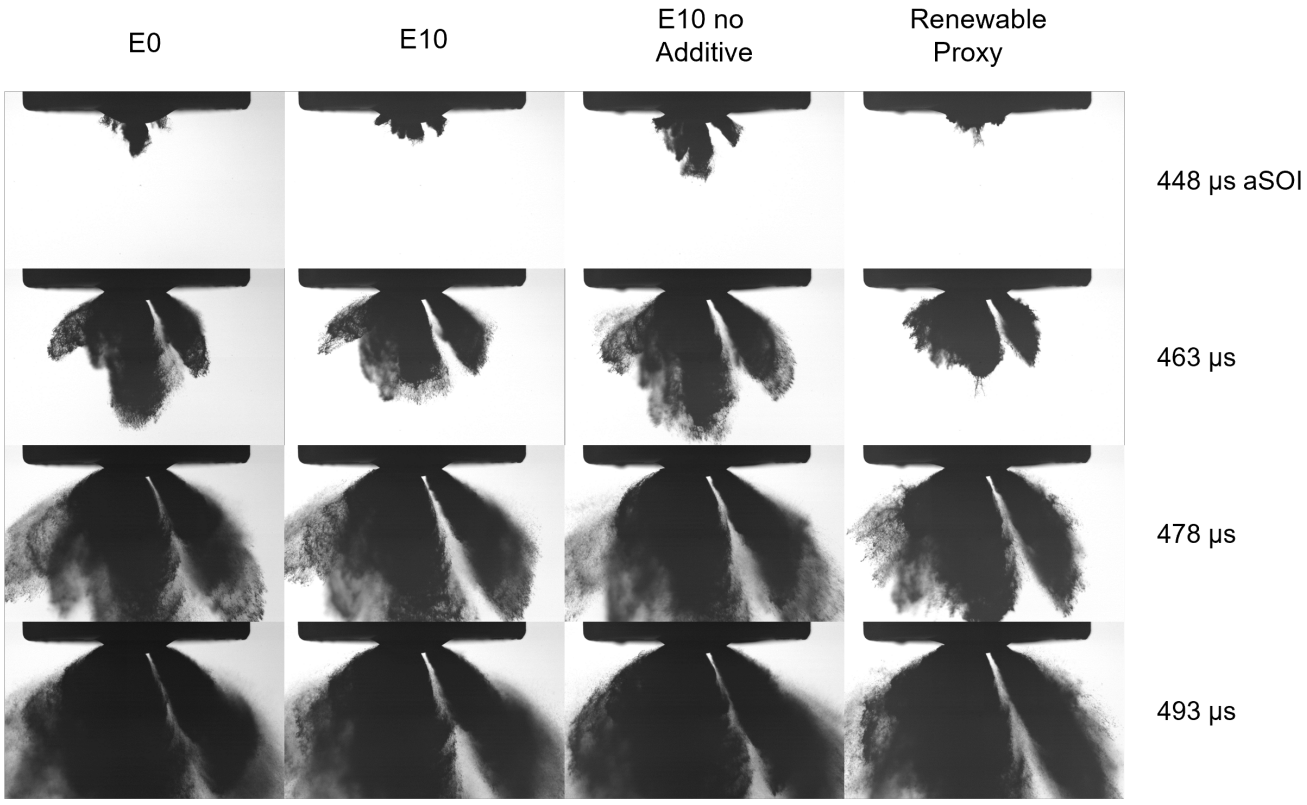

(a) Start of Injection

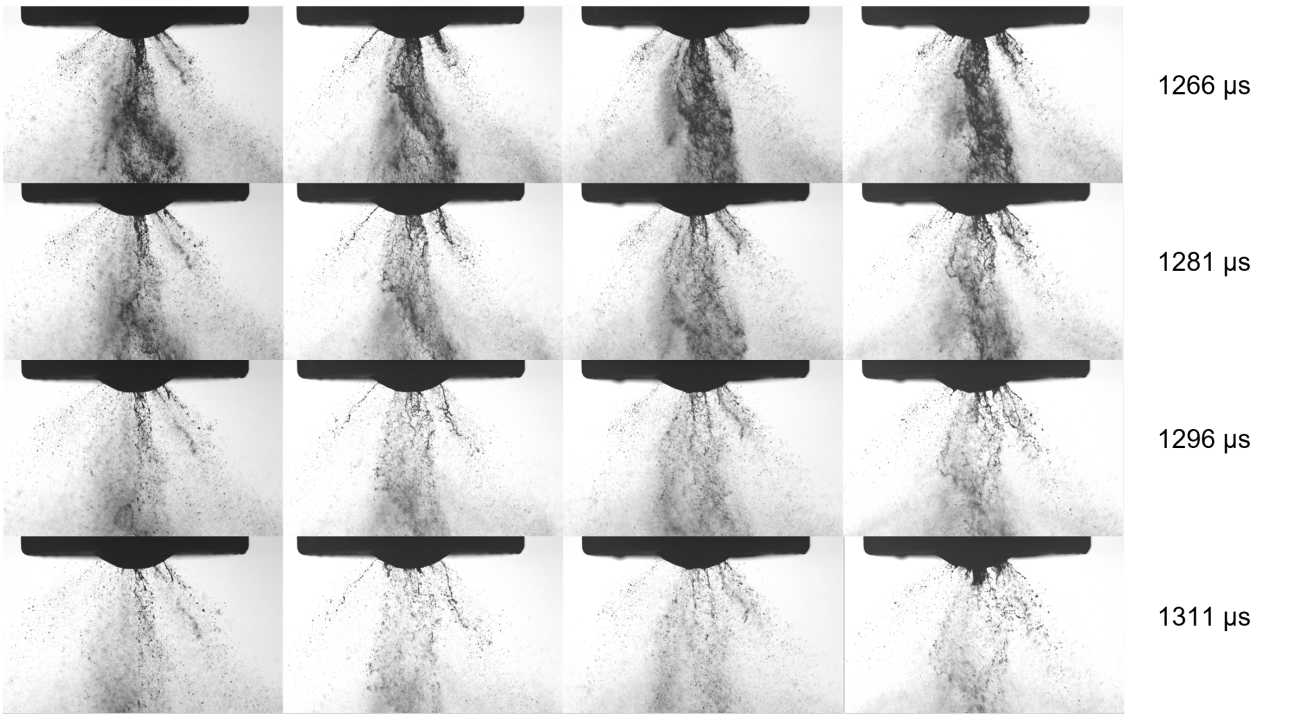

(b) End of Injection

Figure 7: Comparison of four test fuels at the start of injection. Frames sequences are synchronised within ±2 µs from the injection trigger for SOI. EOI frames are synchronised off of the needle bounce which was evident in each spray event recorded, as such timings given are ±30 µs across a row

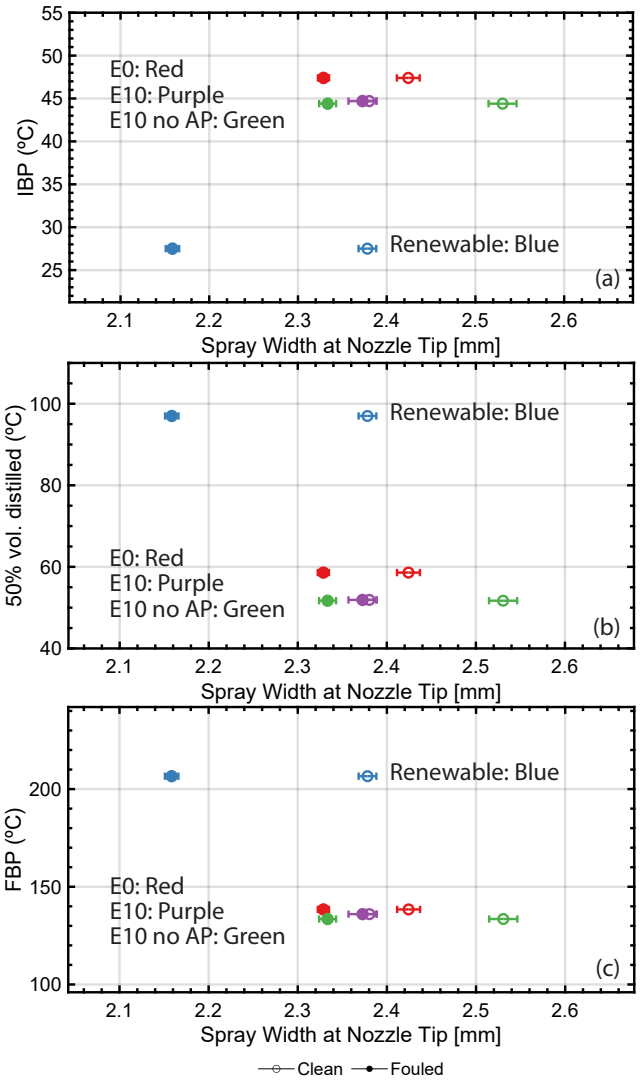

Figure 8: Influence of fuel distillation properties and injector nozzle fouling on the spray width at the nozzle tip. Data points shown are for both clean (open dots), and fouled (filled dots) injector types with the fuel colour code being given described with labels that are inline with the data points

One explanation for this could be that, the significantly higher density gives more momentum to the liquid core, therefore effectively preventing it from penetrating axially as the ethanol fuels do. A second explanation is that the lower viscosity would likely have a significant impact on the fuel spray and nozzle surface interactions, decreasing the spray angle of the plume and therefore reducing axial penetration. Figure 7b shows a qualitative sequence of fuel sprays at the end of injection from the same recordings as the sequences shown at SOI in Figure 7a. These sequences were synchronised by the needle bounce, which occurred in almost all of the spray events recorded. Looking at the first row in Figure 7b, the ethanol fuels appear to be more evenly distributed across the field of view, with the liquid core for the renewable proxy appearing much denser. The denser renewable fuel is likely a result of the higher distillation characteristics shown in Table 2 and the density causing the majority of the spray to have a downward momentum rather than an axial one. The second, third and fourth rows in Figure 7b demonstrate similar spray patterns and continue on the characteristics described in the first row. These similar spray patterns are except for the renewable proxy, which appears to show slightly larger ligaments than the ethanol fuels, with the ethanol fuels with the typical GDI additive showing slightly longer ligaments. The size has not been measured as ligament and drop sizing is outside the scope of this article and would require further investigation to confirm. Figure 9, shows a series of plots providing quantitative results from the processing algorithm described in the methods section.

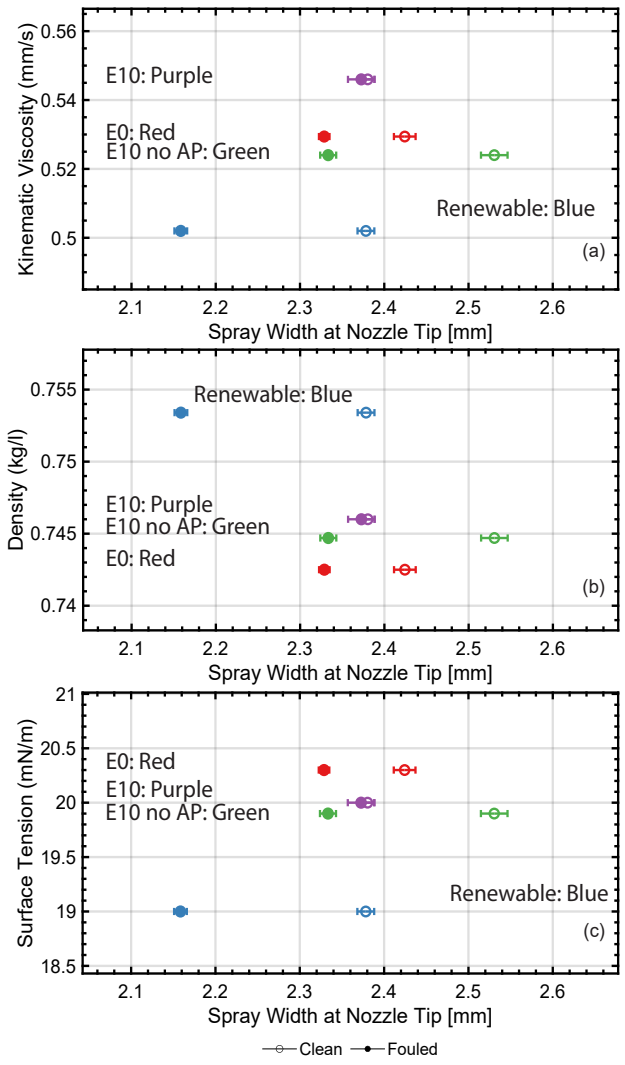

Figure 9: Influence of physical properties on spray width at the nozzle tip, using the clean fuel injector. Test conditions in this figure are 200 bar injection pressure and 1000 mbar ambient pressure with chamber and nozzle temperature set to 333 K. Data points shown are for both clean (open dots), and fouled (filled dots) injector types with the fuel colour code being given described with labels that are inline with the data points

As such, the plots in Figures 8 and 9 show trends between the spray width at the nozzle tip compared to a property which was measured for each fuel, where the mean measurement is represented by a marker and the standard error of the mean is represented by error

bars. One observation is that the E10 and E10 without additives has a very minimal effect on these fuels' initial, 50% and final boiling points, often leaving a large gap in the measurement plots. Despite this, the initial signs indicate that the correlation starts positive for spray width with Figure 9a, showing a positive linear trend between IBP and spray width at the nozzle tip for the fouled injector. However, the trend for the same measurement on the clean injector is not as clear, suggesting that distillation has a more greater influence as injector deposits begin to develop. As for 50% distillation and FBP shown in Figures 9b and c, a negative linear trend between these properties and spray width at the nozzle tip was found, with essentially no trend apparent for the clean injector. It is evident when looking at Figures 8 and 9 that fouling resulted in a reduction in spray width and the injector nozzle tip, with significant differences for all fuels except the E10 fuel. Figure 8a demonstrates a positive correlation between the spray width at the nozzle tip. This relationship was initially unexpected as a lower IBP would lead to a faster boiling, more expansive spray. However, when we compare the result for the renewable fuel to the measured distillation properties given in Table 2, we find that this result is likely due to a sharp rise in distillation temperature between 0 and 50% when compared with the ethanol fuels. This sharp rise indicates it is likely one small volume of a component boiling off at the IBP and, therefore, would not cause a significant expansion leading to a wider spray. The same can be said for the other tested fuels. However, due to their more tightly grouped distillation characteristics, the difference in width measurement is minimal. Figure 8 demonstrates the influence of 50% distillation and FBP on the spray width at the nozzle tip. As previously mentioned, this is expected due to the lower the 50% distillation temperature; it is more likely that the lower half of the distillation curve will be boiling and expanding, producing a wider spray. Figure 9 shows the influence of surface tension, kinematic viscosity and density of spray width at the nozzle tip in both the clean and fouled injectors. This subsequently leads to larger fluid structures that are still attached to the injector surfaces and have increased inertia, resulting in a wider spray plume as shown in Figure 9c. Figure 10 and 11 show the influence of fouling, fuel distillation and fluid properties on the spray angle in the near nozzle region. Firstly Figure 9a shows the influence of viscosity on spray width at the nozzle tip and a positive correlation. This result is generally expected as the viscosity will alter how the flow interacts with the nozzle geometry.

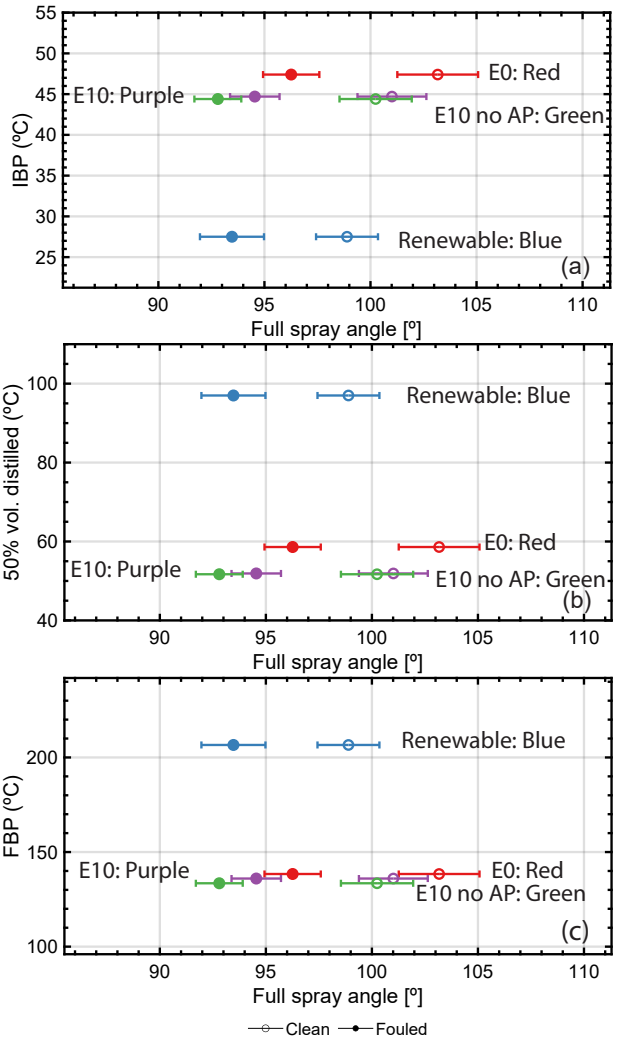

Figure 10: Influence of fuel distillation properties and injector nozzle fouling on the spray spray in the near nozzle region. The error bars on the plot represent the standard error of the mean computed with 20 experimental repeats for the clean injectors and 10 for the fouled. Data points shown are for both clean (open dots), and fouled (filled dots) injector types with the fuel colour code being given described with labels that are inline with the data points

More viscous fluids will drag more on the internal injector surfaces and counter-bore, increasing the spray width which is consistent with results seen in [8, 9]. This viscous friction effect is further exacerbated by surface tension; the higher the surface tension the more resistant a fluid will be to break up. In these measurements, it is clear the fouling reduces the spray angle, which along with the result of fouling, also decreases spray width, as shown in Figures 9 and 8 would suggest an increase in overall penetration by proxy, however the field of view of the experimental setup is not large enough to determine this accurately. As for an influence on fluid properties or distillation characteristics, surface tension, density and IBP are the only physical properties to demonstrate any noticeable trend, with IBP and surface tension both demonstrating positive trends for both clean and fouled injectors, whereas density shows a slight negative trend for both injectors.

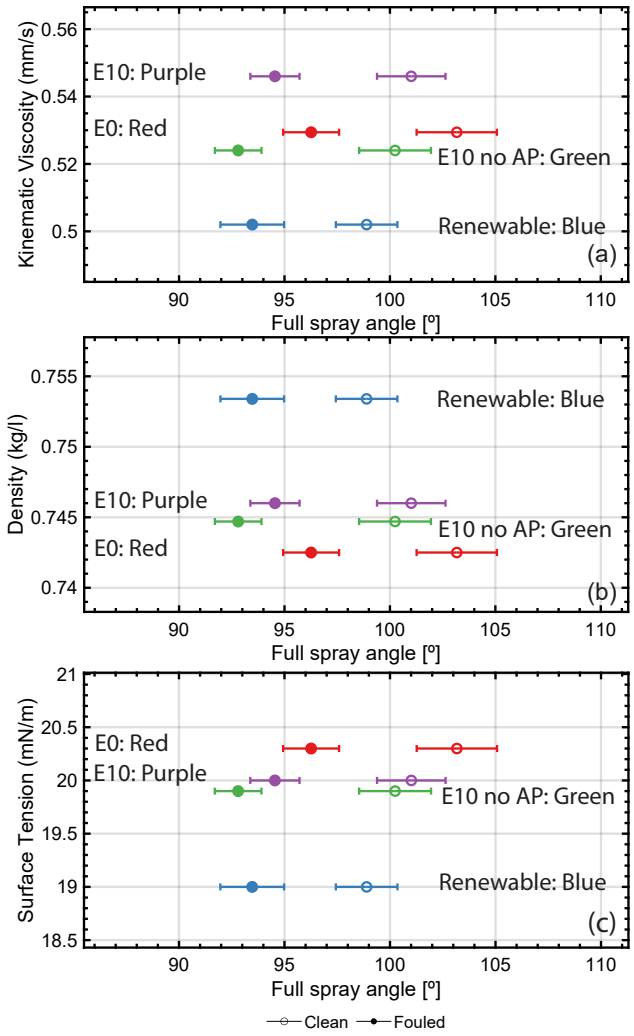

Figure 11: Influence of fuel physical properties and injector nozzle fouling on the spray spray in the near nozzle region. The error bars on the plot represent the standard error of the mean computed with 20 experimental repeats for the clean injectors and 10 for the fouled. Data points shown are for both clean (open dots), and fouled (filled dots) injector types with the fuel colour code being given described with labels that are inline with the data points.

CONCLUSION

This study aimed to provide insights into the impact of fluid properties and fouling on spray characteristics in GDI fuel injection systems. In summary, four gasoline fuels were used with high-speed microscopic shadowgraphy measurements to investigate the near nozzle region. The key findings from this research can be summarised as follows:

- A significant impact from fouling at the start and end of injection (SOI and EOI) was observed, with fouling inhibiting atomization and producing larger ligaments at EOI.
- Ethanol fuels (E10) demonstrated a more even distribution than E0 and renewable proxy, which can be attributed to their distillation characteristics.
- The renewable proxy resulted in a smaller dispersion angle, potentially due to its higher density and lower viscosity.
- A MATLAB processing algorithm was employed to measure spray width and angle, revealing trends between physical fluid properties and spray characteristics.
- Positive trends were found between viscosity, surface tension, and initial boiling point (IBP) with spray width at the nozzle tip. Conversely, negative trends were observed for 50% distillation, final boiling point (FBP), and density.
- Despite a higher standard error of the mean for spray angle measurements, a consistent 5 degrees difference between clean and fouled injectors was deemed significant.

It is important to note that the current dataset is limited, and further investigations with a larger dataset are necessary to validate and expand upon these findings. In future studies, researchers should seek to corroborate the trends observed in this research and explore additional factors that may influence the spray characteristics of GDI fuel systems.

ACKNOWLEDGEMENTS

This work was supported by the UK's Engineering and Physical Science Research Council [EPSRC grant EP/S513751/1] and BP International Ltd.

REFERENCES

[1] S. Shuai, X. Ma, Y. Li, Y. Qi, and H. Xu, "Recent progress in automotive gasoline direct injection engine technology," *Automotive Innovation*, vol. 1, no. 2, pp. 95–113, 2018. [Online]. Available: https://doi.org/10.1007/s42154-018-0020-1

[2] R. Smocha, D. Vuilleumier, K. Christison, P. Loeper, N. Ketterer, L. Pickett, J. Hwang, N. Kim, and T. Strickland, "Gasoline direct injector deposits: Impacts of fouling mechanism on composition and performance," *SAE International Journal of Advances and Current Practices in Mobility*, vol. 4, no. 4, pp. 1413–1430, 2022. [Online]. Available: https://doi.org/10.4271/2022-01-0488

[3] Z. Yue and S. Som, "Fuel property effects on spray atomization process in gasoline direct injection," 2020. [Online]. Available: https://doi.org/10.4271/2020-01-0329

[4] C. Jiang, H. Xu, D. Srivastava, X. Ma, K. Dearn, R. Cracknell, and J. Krueger-Venus, "Effect of fuel injector deposit on spray characteristics, gaseous emissions and particulate matter in a gasoline direct injection engine," *Applied Energy*, vol. 203, pp. 390–402, 2017. [Online]. Available: https://www.sciencedirect.com/science/article/pii/S0306261917307614

[5] H. Song, J. Xiao, Y. Chen, and Z. Huang, “The effects of deposits on spray behaviors of a gasoline direct injector,” *Fuel*, vol. 180, pp. 506–513, 2016. [Online]. Available: https://www.sciencedirect.com/science/article/pii/S0016236116302320

[6] S. Henkel, Y. Hardalupas, A. Taylor, C. Conifer, R. Cracknell, T. K. Goh, P.-B. Reinicke, M. Sens, and M. Rieß, “Injector fouling and its impact on engine emissions and spray characteristics in gasoline direct injection engines,” *SAE International Journal of Fuels and Lubricants*, vol. 10, no. 2, pp. 287–295, 2017. [Online]. Available: https://doi.org/10.4271/2017-01-0808

[7] R. Lindgren, M. Skogsberg, H. Sandquist, and I. Denbratt, “The influence of injector deposits on mixture formation in a disc si engine,” *SAE Transactions*, vol. 112, pp. 852–861, 2003. [Online]. Available: http://www.jstor.org/stable/44742314

[8] H. Ulrich, B. Lehnert, D. Guénot, K. Svendsen, O. Lundh, M. Wensing, E. Berrocal, and L. Zigan, “Effects of liquid properties on atomization and spray characteristics studied by planar two-photon fluorescence,” *Physics of Fluids*, vol. 34, no. 8, p. 083305, 2022. [Online]. Available: https://aip.scitation.org/doi/abs/10.1063/5.0098922

[9] L. Zigan, J.-M. Shi, I. Krotow, I. Schmitz, M. Wensing, and A. Leipertz, “Fuel property and fuel temperature effects on internal nozzle flow, atomization and cyclic spray fluctuations of a direct injection spark ignition–injector,” *International Journal of Engine Research*, vol. 14, no. 6, pp. 543–556, 2013. [Online]. Available: https://journals.sagepub.com/doi/abs/10.1177/1468087413482320

CONTACT

Corresponding author: c.crua@brighton.ac.uk

DEFINITIONS, ACRONYMS and ABBREVIATIONS

GDI - Gasoline Direct Injection
PFI - Port Fuel Injection
BSI - Back Side Illuminated
IBP - Initial boiling point
FBP - Final boiling point
SOI - Start of injection
EOI - End of Injection
LES - Large Eddy Simulation
VOF - Volume of Fluid